Helium tribology of Inconel 617 subjected to laser peening for high temperature nuclear reactor applications

Vasilis Tsigkis[1], Md Saifur Rahman[1], Lloyd Hackel[2], Keivan Davami[3], Ali Beheshti[4*], Andreas A. Polycarpou[1**]

[1] J. Mike Walker '66 Department of Mechanical Engineering, Texas A&M University, College Station, TX, USA.
[2]Curtiss Wright Surface Technology, Livermore, CA, USA.
[3] Department of Mechanical Engineering, The University of Alabama, Tuscaloosa, AL, USA
[4] Department of Mechanical Engineering, George Mason University, Fairfax, VA, USA.

[*] Co-corresponding author. Tel.: +1 703 993 5836; fax: +1 703-993-5383.
E-mail address: abehesh@gmu.edu (A. Beheshti).
[**] Corresponding author. Tel.: +1 979 458 5763; fax: +1 979 845 3081.
E-mail address: apolycarpou@tamu.edu (A.A. Polycarpou).

Abstract*: Inconel 617 is among the best candidates for utilization in high temperature gas cooled reactor tribo-components. However, the combined effects of sliding contact, along with intermittent idle times and very high temperature material degradation, deteriorates the alloy tribological performance, especially under a helium atmosphere. Laser peening is a surface treatment technique which can enhance the properties at the surface and subsurface by generating deep residual stresses and enhanced microstructure. Herein, we report the tribological behavior of regular laser peened as well as thermally-engineered laser peened Inconel 617 under helium and air atmospheres at 800°C. In addition to friction and wear studies, the specimens are characterized by different analytical techniques to further understand the mechanisms involved in the peening process and sliding contact. Regardless of the peening process and post-process treatment types, it is observed that laser peening improves the tribological characteristics of Inconel 617. Interestingly, laser peening followed by helium thermal aging shows highly enhanced tribological behavior. This is attributed to the strengthening effect of the laser peening on the surface oxides providing an excellent and lasting protective and lubricating film under helium exposure.*

Keywords

High temperature tribology; Inconel 617; Laser peening; Thermal microstructure engineering;

Helium thermal aging.

1. Introduction

Increasing demand for electricity production, coupled with increasing regulations for clean and reliable energy, have resulted in extensive research and development in nuclear power production during the past decade. The Generation IV International Forum has launched promising nuclear energy system concepts, seeking more sustainable, reliable, and efficient power plants [1]. A very-high temperature reactor (VHTR) and a high-temperature gas-cooled reactor (HTGR) are among the selected candidates to operate at high outlet temperatures (above 750°C) designed to reach 60-year operational lifespan [2]. Although helium (He) is an inert gas, it inevitably contains impurities resulting in accelerated surface degradation for mechanical components in coolant circulation systems [3]. Besides exposure to harsh VHTR and HGTR environments, tribological parts in these reactors, in particular, undergo low speed sliding (e.g., valves and control rods under intermittent oscillatory motion and often combined with long idle times), or high frequency small vibratory condition (e.g., fretting in heat exchanger joints). Accordingly, their contact behaviors are of vital importance in maintaining reactor stability and operational integrity [4].

Inconel 617 (Ni-Cr-Co-Mo solid solution alloy, referred to as INC 617, hereinafter) and Incoloy 800HT or alloy 800HT (Ni-Fe-Cr austenitic solid solution alloy) are the main structural candidates for the construction of key components in VHTR/HTGR, due to their exceptional strength and corrosion resistance [4,5]. Furthermore, the literature is abundant with studies that show these alloys to have superior oxidation and creep resistance, thermal fatigue performance, and phase stability [6-14]. Comprehensive comparative high temperature (HT) tribological studies in He and air environments were carried out on both alloys depicting that INC 617 outperforms alloy 800HT, in terms of tribological performance [2,4,15,16]. Still, the tribological studies of INC 617 at HT under nuclear reactor He environment showed high friction [17,18]. It was revealed that the

absence of a mitigating compacted, and stabilized oxide layer leads to direct contact between metallic surfaces exposed to He environment promoting high friction and accelerated surface degradation and wear. Also, under HT He environment, INC 617 experiences a significant degradation of its mechanical properties (i.e., modulus and hardness) [19] that can result in accelerated wear and higher friction.

Although the widely used engineering technique of surface coatings can be developed to alleviate the friction and wear issues in reactor components, this should be the last resort as it can introduce other complexities in the reactor systems that require very high reliability and system integrity. This calls for a robust surface engineering technique that can enhance the tribological behavior and potentially other mechanical properties (e.g., creep and surface fatigue) and at the same time does not have regulatory concerns (as compared to, for example, to coatings as separate materials). Laser Peening (LP) is among those robust surface engineering techniques which induces high strain rate (up to 10^{-7} s^{-1}) plastic deformation on the surface (and deep into the subsurface), by means of short duration laser pulses (**Fig. 1**). Several mechanisms are in play during LP, for example the generation of high density tangled dislocations, and beneficial phase transformations, which generally result in high intensity compressive residual stresses, refined microstructures, and hardened regions for various alloys. It should be noted, however, that the surface modification benefit of LP is material dependent. For example, Kanjer et al. and Lavisse et al. reported negligible hardening effects on titanium and its alloys [20-22]. For the material studied here, there exists no report in the open literature on the effect of LP on INC 617 microstructure. Nonetheless, for superalloys with close microstructure to INC 617 such as INC 625 and INC 718, previous studies showed that LP generates promising structural modifications, compressive residual stresses and consequent hardening [23-26]. LP has also been proven to enhance corrosion resistance,

fatigue life, and fracture resistance of INC 600 and INC 718 [27,28]. While the literature is abundant on the beneficial contribution of LP on the tribological performance of metallic surfaces, for example aluminum, magnesium, titanium and steel alloys [29-34], limited works are focused on nickel-based alloys [35,36]. In addition, no report exists in the open literature on the effect of LP on INC 617 friction and wear.

The successful implementation of LP in HT applications is, however, challenging due to diminishing effect of LP because of thermal relaxations and microstructure modifications at elevated temperatures manifesting as defect annihilation and recovery, grain boundary migration, phase coarsening, and phase dissolution [37-40]. The relaxation of the LP induced stresses and microstructures at elevated temperatures is driven by the material softening (thermal mechanism), and external stresses coupled with the internal stresses of the material which can act synergistically and induce plastic deformation (mechanical mechanism), or the combination of both [38]. For nickel-based superalloy, however, LP showed relatively good thermal stability and longer lasting effectiveness which makes it a potential for HT applications [25,40,41]. Munther et al. showed that the combination of cyclic thermal annealing and LP, called thermal microstructure engineered (TME) LP, substantially increases the thermal stability of LP induced microstructure in additively manufactured Inconel 718 after exposing the treated specimen to 600°C up to 350 hours. The repeated strain input achieved through cyclic LP and intermittent heat treatments encouraged the formation of γ' and γ'' phases which contributed in stabilizing the microstructures induced after the LP process [37].

The effects of LP on the tribological performance of several materials have been studied in the literature [29,30,32,34], and a decreasing trend of both friction and wear values of the treated

specimens, compared to the as-received (untreated) specimens was observed. Regarding HT applications, Tong et al. investigated the tribological characteristics of LP specimens, by performing HT tribo-testing (up to 600°C) in an open environment utilizing a titanium alloy (TC11). Their findings pointed towards a lower degree of thermal softening of the subsurface, which was able to maintain the integrity of the superficial oxide tribo-layer, and lower friction and wear were reported [43]. In spite of potential application of LP in enhancing the tribological behavior of superalloys, there are no studies on their tribological performance especially at HT. Also, the impact of LP+TME on friction and wear has yet to be explored, regardless of the surrounding environment and temperature.

Herein, we report the tribological behavior of INC 617 at an extreme temperature of 800°C under HTGR (99.999% He) environment following LP, and cyclic LP with intervening TME. Also, we simulate thermal aging under reactor conditions, by exposing the LP specimens in a HT (950°C) He environment to further study of how LP and TME processes affect the surface microstructure and the frictional/wear performance after aging.

2. Experimental procedure

2.1 Materials

Disk specimens with dimensions of 25.4 × 25.4 × 15 mm as well as 19 mm long hemispherically tipped pins with tip radius of 8.15 mm were machined from INC 617 plate, provided by Idaho National Laboratory (INL). The chemical composition of INC 617 is presented in **Table 1**. The high concentration of nickel and chromium provide good oxidation resistance at HT, while chromium, cobalt, and molybdenum are the hardening/strengthening agents, which are dissolved into the solution matrix. After the LP and TME processes, the disks were polished down to 80 ± 5 nm root mean square (rms) roughness using a sequence of 600, 800, 1200, and 2400 abrasive pads

with a minimal layer removal. This was also followed by polishing with a 3 μm diamond suspension, and a final pass with a 0.05 μm colloidal silica. During the LP process and due to high local temperatures, a thin recast layer is formed on the surface. Also, during TME (600°C in air), the surface is subjected to some degree of oxidization. For example, Gill et al. demonstrated that a recast layer of ~5 μm in thickness was formed on the surface of INC 718, after the LP process without a protective layer [23]. Depending on the LP process (laser energy, cycles, etc.), CWST measurements after LP and LP+TME, showed oxide layer in the range of 5 to 20 μm for nickel-based superalloys. For consistency, in tribological tests and to eliminate the effect of this LP process-based transient layer and its material and topography, samples LP-R and LP-TME were subjected to polishing, as explained above. Commercial abrasive pad polishing is a standard procedure after LP process. The samples were also sporadically examined during polishing, and the procedure was terminated as soon as the surface oxides were completely removed and were not optically visible on the surface. Also, optical microscopy was employed to further examine the polished surface to ensure no recast/oxide layer was present. Herein, polishing removed a layer thickness of 30 to 40 μm. It should be added that samples subjected to He aging were not polished following the aging process, however, they were polished prior aging.

Table 1. *Chemical composition of INC 617 provided by the manufacturer (units are in wt.%).*

Nickel	**Chromium**	**Cobalt**	**Molybdenum**	**Aluminum**	**Carbon**	**Iron**
53.27	22.02	11.91	9.38	1.1	0.08	1.46
Manganese	**Silicon**	**Sulfur**	**Titanium**	**Copper**	**Boron**	**Phosphorous**
0.23	0.2	0.001	0.32	0.02	0.002	0.005

2.2 Laser Peening and TME

A schematic of the LP process is illustrated in **Fig. 1**, wherein water was used as a confinement medium. The LP process was performed without a protective coating. However, the recast layer

was removed with a very light polishing using 3M Scotch-Brite after the process. Fresh INC 617 disks were subjected to the LP process with a beam irradiance of 7 GW/cm^2. To achieve that, a 1056 nm flash pumped Nd glass laser was used delivering 13 J per pulse on target. The spot size was 9 mm^2 square with 3% spot-to-spot overlap providing true 100% coverage for each layer. Laser pulse duration of 18 ns (full width half height) and 0.7 ns rise time were used. For preparation of regular LP specimens (symbolized by LP-R), the INC 617 disks were subjected to a 4-layer LP without an intervening TME or a post-treatment process. Regarding the LP annealed specimens (LP-TME), a combination of LP and intervening thermal treatment was carried out. Specifically, a sequence of 3 LP/TME processes was followed by a final LP, resulting in 4 LP events and 3 intervening TME surface treatments. Identical LP process parameters were used compared to LP-R samples, and each intermittent TME was carried out at 600°C (roughly 55% of material melting temperature, T_m) for 8 hours in air. The LP and TME treatments were performed with state-of-the-art laser and robotic positioning systems available at Curtiss Wright Surface Technologies (CWST), California, USA. Furthermore, some of the LP-R, and LP-TME, as well as INC 617 specimens were subjected to post-treatment thermal aging simulating HTGR/VHRT reactor environment, resulting in additional sample types referred to as LP-A, LP-TME+A, and INC 617-A (aged INC 617 with no peening), respectively. Details of the aging procedure are presented in the next section.

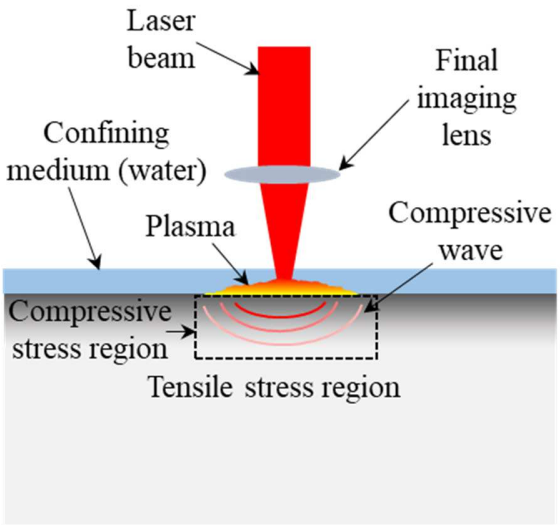

Fig. 1. *Schematic representation of LP process.*

2.3 Post-treatment aging

In an effort to simulate long-time exposure of the tribological components under HTGR/VHRT conditions, an aging process was implemented, following the LP and TME treatments. In the present study, He with purity of 99.999% was used where the concentration of the impurities, in parts per million (ppm), is as follows: O_2 (1), H_2O (1), total hydrocarbons, i.e., CH_4 (0.5), CO (1), CO_2 (1), and N_2 (5). These impurity levels are similar to the cooling medium of VHTR [3]. To assure the minimum presence of oxygen within the furnace, a vacuum/flashing protocol was used (see Ref. [44] for details). Afterwards, the furnace was set to the target temperature of 950°C, with 6°C/min ramping temperature, followed by constant temperature aging time of 10 hours. The samples were then cooled down to ambient temperature with a rate of 1°C/min or less. A constant He flow rate of 0.14 m^3/hour was maintained during heating, aging, and cooling.

2.4 High temperature tribometer

A versatile custom-built HT Tribometer (HTT) shown in **Fig. 2** was utilized in this study which allows in-situ tribological experiments in a wide range of temperatures, from -196 to 1000°C,

under different atmospheres (including N_2 and He). A pin-on-disk configuration (**Fig. 2(c)**) with a mean wear track diameter of 17.5 mm was used. Detailed information on the HTT can be found elsewhere [15].

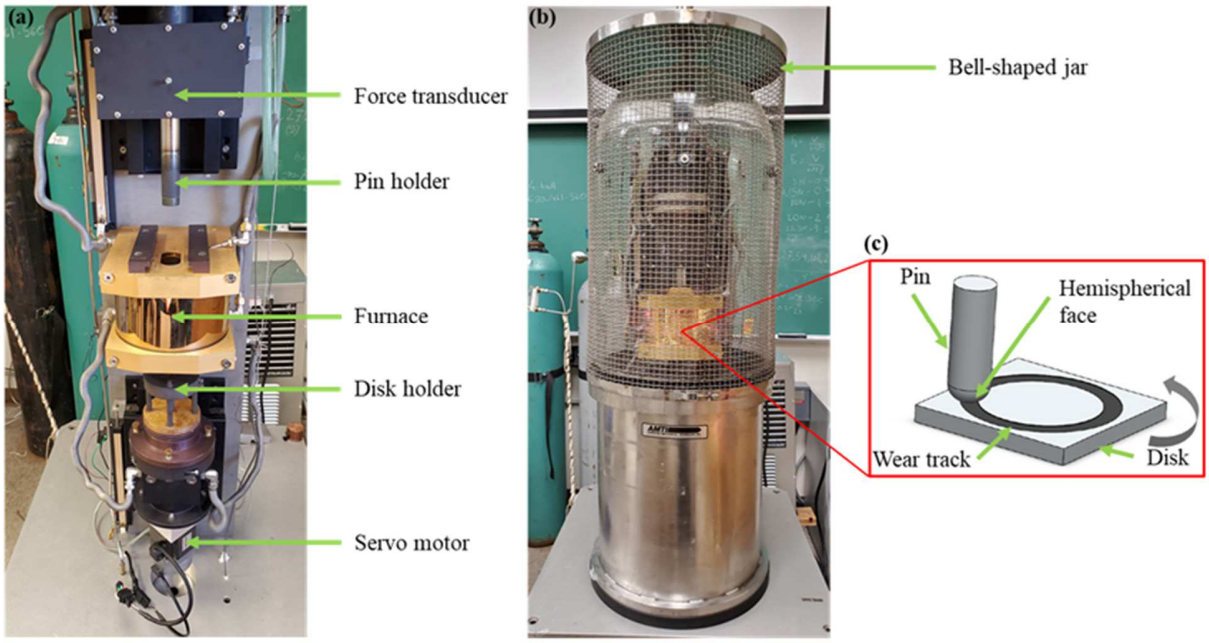

Fig. 2. *Experimental setup: (a) photograph of HTT, (b) bell-shaped jar enclosure, and (c) pin-on-disk configuration.*

2.5 Experimental conditions

The experimental conditions are outlined in **Table 2**. Five different tribo-pairs were selected to investigate the contribution of LP, TME and post processes (aging) on INC 617 tribological performance. All tribo-pairs were constituted of an untreated INC 617 pin vs. different sample types, namely INC 617, INC 617-A, LP-R, LP-TME, LP-A, and LP-TME+A disks, and the resulting tribo-pairs are named as such for convenience. To have a better comparison and to further understand the involved wear and friction mechanisms, in addition to He environment, limited tribological tests were also performed in air. The linear velocity was set to 0.4 m/s, with a 30-

minute duration resulting in 72 m sliding distance. The untreated INC 617 served as the baseline to gauge the effect of each treatment on the tribological behavior of the tribo-pairs.

For the experiments under He environment, a vacuum-flashing protocol was used to ensure minimum presence of contaminants within the chamber/jar, as detailed in Ref. [15]. Thereafter, the furnace was heated up to 800°C. During the experiment, the pressure was controlled at 0.1 ± 0.02 psi (gage). After the end of the experiment, the samples were let to cool in He with a continuous flow of 0.14 m^3/hour. A minimum of three experiments for each tribo-pair were carried out to assure repeatability.

Table 2. *Experimental conditions.*

Samples		**Temperature**	**Load (Initial Hertzian pressure)**	**Sliding Speed**	**Sliding Distance**	**Ambient**
Pin	***Disk***					
INC 617	INC 617	800°C	5N (580.7 MPa)	0.4 m/s	72 m	He
	INC 617-A*					He
	LP-R**					He
	LP-TME***					He, Air
	LP-A					He, Air
	LP-TME+A					He, Air

**A: aged; **R: regular peened with no TME or aging; ***TME: thermally engineered*

2.6 Characterization

Microhardness measurements were carried out using a Vickers microhardness tester (Wilson TUKON 1102) to measure the surface hardness following the LP and TME processes, and after aging. Investigation of the pin and disk worn surfaces following tribo-testing was carried out with an Olympus DSX510 optical microscope. A JEOL JSM-7500F Scanning Electron Microscope (SEM) was employed to explore the topography of the unworn and worn areas of the untreated and treated disks. Cross-sectional SEM and Energy Dispersive Spectroscopy (EDS) analysis of the unworn and worn surfaces were also performed to analyze the near surface oxide morphology and elemental composition. Transmission Electron Microscopy (TEM, Fei Tecnai F-20) foils were

sectioned from the top (treated) surfaces through focused ion beam (FIB) milling. Foils were approximately 10 μm long and 5 μm wide, encapsulating the upper affected region of the material. A Dektak (Bruker) stylus profiler was used to measure the wear rate of the disks.

3. Results and Discussion

3.1 Microhardness

Surface hardening is achieved by the high strain plastic deformation induced by the laser pulses, which result in an increase in the dislocation density, the generation of compressive stresses, and grain refinement [23,25,45]. The microhardness values of the disk specimens are depicted in **Fig. 3**. Note that the penetration depth was maintained at 8-12 μm in all specimens to assure that the hardness levels of the specimens corresponded to the upper surface and well within the LP regions. It should be emphasized, nevertheless, that LP can induce surface modifications which result in considerably hardened regions. For instance, for INC 718, surface modifications more than ~500 μm depth, was reported [23]. The untreated INC 617 features the lowest microhardness value of 190 HV or 1.86 GPa. After 4 passes of LP the average surface microhardness experiences a 62% increase resulting in 3.03 GPa, confirming a successful implementation of LP in enhancing the microhardness of the treated sample (LP-R). The TME process (LP-TME) results in an additional increase on the average surface microhardness (7% at 3.22 GPa), compared with LP-R. It is noted that the LP-TME sample was polished after the LP+TME processes to remove any surface oxides formed when exposed at 600°C during TME.

The effect of LP+TME process on the surface enhancements of INC 718 was studied by Palma et al. and Munther et al. and was elucidated that the increase in hardness is related to a combined effect of precipitation hardening and microstructure pinning effect [37,42]. Generally, precipitation hardening of INC 617 is induced at temperatures of 650 to 760°C, by γ' and γ'' phases,

respectively. With the current TME procedure (600°C-8 hours), mild strengthening is expected, which is mainly attributed to the formation of fine γ′ particles [42]. More importantly, it is shown that cyclic LP and the subsequent plastic deformation can encourage the formation of γ″ phases at lower temperatures (650°C), that will cause a further increase in the material's hardness [37].

The LP specimens were also subjected to a post-aging thermal treatment of 950°C for 10 hours in He. LP-A and LP-TME+A appear to have similar microhardness enhancements, as LP-TME, showing after 10 hours of very high temperature aging, the LP effect was still preserved. It should be noted, however, that the microhardness values of LP-A, and LP-TME+A are also affected by superficial oxides (3-6 μm thick) following exposure at 950°C in He atmosphere (please see section 3.5 for cross-section EDS). Microhardness measurements of untreated INC 617-A show that the surface oxides increase the microhardness by 65%, compared to the unaged INC 617 specimen. Salari et al. measured the nanohardness of surface oxides (mainly Cr_2O_3) formed on He aged INC 617 by nanoindentation and reported high hardness values of 25 GPa at depth up to 200 nm [13]. Nevertheless, the indentations performed herein penetrated through the few microns-thick oxide layer, targeting the subsurface and as a result the effect of generated hard oxides on microhardness findings was reduced. The LP aged samples (LP-A, LP-TME+A) demonstrate a 17% higher microhardness value than INC 617-A, thus the further increase in hardness can be mostly attributed to LP and TME processes than the aging process. As depicted in **Fig. 3**, by exposing the specimens to the VHTR/HTGR environment (950°C under He) for 10 hours, defect annihilation and thermal relaxation is prevented, and the microhardness values are retained. Note that the thermal stability of LP specimens at long HT exposures does not fall into the scope of this study, nonetheless, to further evaluate the microstructural stability of LP and LP+TME processes, longer thermal exposure (60 hours) was performed followed by TEM imaging (see next section).

It is, however, noted that the current study focuses on the tribological behavior of INC 617 treated by LP under VHTR/HTGR environments.

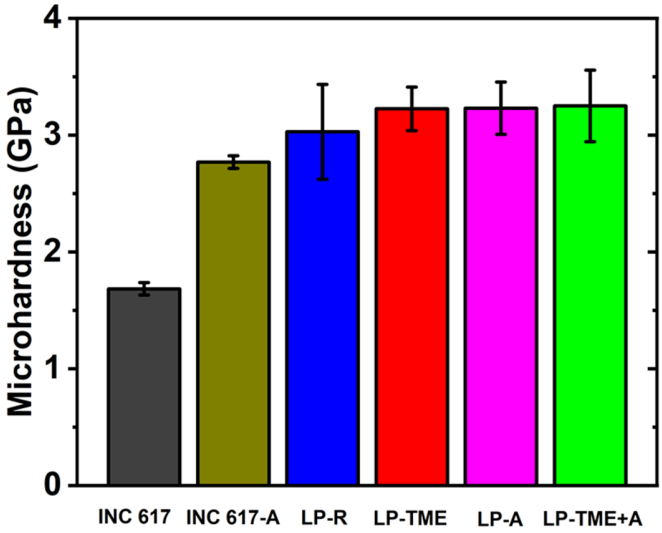

Fig. 3. *Surface microhardness values measured by Vickers indentation of the as-received disk specimens before HT sliding. Error bars designate ± 1 standard deviation.*

3.2 TEM after LP and LP+TME processes

LP and especially LP+TME processes provide enhanced microhardness results on treated INC 617. In this section, TEM imaging was performed to evaluate the stability of LP induced microstructures after long time HT exposure. Both LP and LP+TME samples were subjected to 60-hour, 800ºC exposure wherein subsequent TEM characterization was carried out. Investigation of the treated surface of the material subject to each of the treatment schemes was carried out to discern relevant microstructural alterations known to play a role in influencing surface-level mechanical properties. Following thermal exposure and 4 subsequent layers of laser peening (LP-R sample), dense dislocation networks are observed occupying the immediate sub-surface, to a depth of 1 μm (**Fig. 4(a)**). Above these dislocation networks, nanoscale subgrain structures are also found to dominate the microstructural changes occurring in the uppermost plastically

deformed regions, occurring to a depth of 300 nm. The presence of subgrains is surmised to be a result of cyclic LP wherein repeated strain facilitates the transformation of defect networks into fine, subgrain structures [46]. With a buildup of sufficiently dense dislocations, defect networks then begin to organize into low energy configurations, or subgrains, under the influence of long-range stresses [47]. This mechanism has been proven to be favorable for the deformed microstructure as it enables further work hardening effects by impeding the motion of glissile dislocations.

Following LP+TME (**Fig. 4(b)**), a similar microstructure is observed. Fine surface-level subgrain is seen with dense, core dislocation networks directly underneath. In this case, the presence of subgrain facilitates the effective "storage" of work hardening effects at HT as defect structures are organized into lower-energy configurations, promoting favorable microstructural and property modification retention when subject to elevated temperature [48,49]. Additionally, nanoscale precipitates are found to be dispersed among surface-level subgrain networks providing another level of stabilization and strength for the deformed microstructure of LP+TME samples. These particles behave as immobile barriers to the motion of strain-driven dislocation motion, and also pin the barriers of newly formed subgrain structures, preventing subgrain coarsening. These findings highlight the stability of the deformed microstructure and provide validity to the LP+TME process and its ability to impart thermally stable microstructural modifications. Typically, near complete defect annihilation would be expected through the use of conventional LP processes, but the addition of cyclic LP and the inclusion of intermittent thermal input promotes work hardening retention through the formation of subgrains and, especially, the precipitation of favorable nanoscale precipitates by modifying their precipitation kinetics. Application of thermal input following LP promotes the preferential nucleation of precipitates along defect sites which acts to

not only strengthen the material matrix, but also provides an additional barrier against thermally activated dislocation motion.

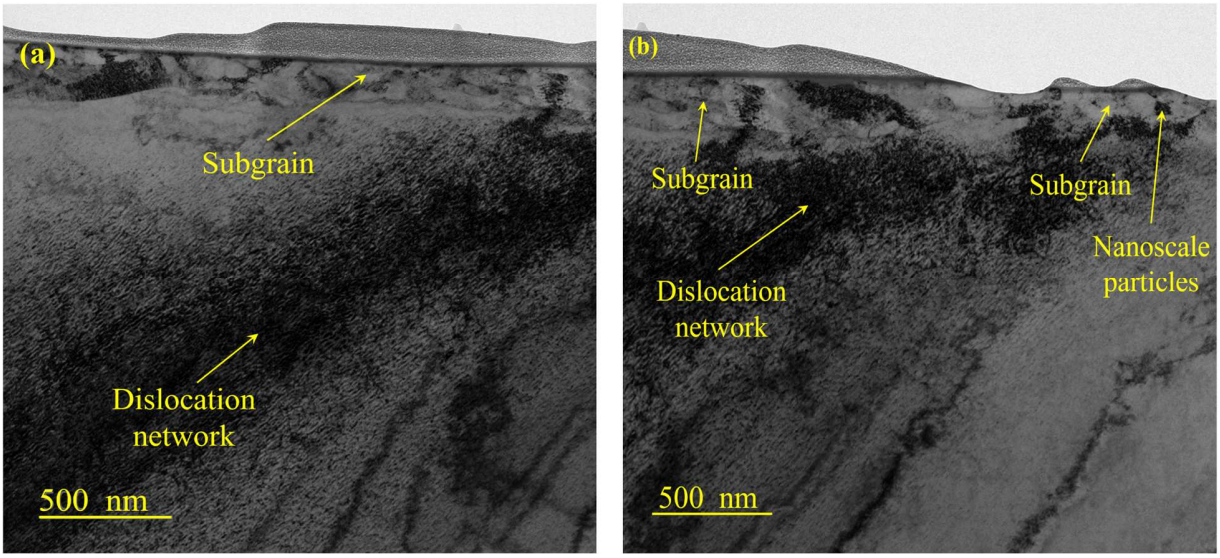

Fig. 4. *TEM micrograph illustrating the microstructure of INC 617 subjected to (a) LP and (b) LP+TME processes after 60-hour thermal exposure at 800°C.*

3.3 Friction and wear

Fig. 5 shows the evolution of the coefficient of friction (COF) under He (**Figs. 5(a)** and **5(b)**) as well as under air environments (**Figs. 5(d)** and **5(e)**) measured for several tribo-pairs under examination. The corresponding average values (**Figs. 5(c)** and **Fig. 5(f)**) are also calculated from the data acquired during the last 40% of sliding distance to minimizing running-in effects. The error bars represent the standard deviation of the mean COF values between repeated experiments. Tribo-pairs INC 617 and LP-R depict similar evolutions of the COF and average values. Noting the error bars, it can be concluded that the effect of LP on steady state HT COF is insignificant. However, LP+TME seems to slightly reduce the COF. The untreated INC 617 was extensively studied by Rahman et al. (800°C, He) and their tribological results are in accord with the present study [15]. INC 617-A (aged in He) appears with high fluctuations in the in-situ COF which result

in an average COF value of 1.17. A complementary experiment was performed with INC 617 aged in air (INC 617-A-Air) to investigate the effect of aging environment on the frictional performance under He environment. It can be seen that during the first cycles of the experiment the COF is low, followed by a rapid increase to a COF of 1.71, due to the deterioration of the integrity of the pre-formed compact oxide layer and the subsequent detachment from the surface. Both LP samples followed by aging process (LP-A, LP-TME+A) feature a dramatic decrease in COF, after a running-in period of high friction and high fluctuations for 25 and 15 m, respectively, resulting in 0.53 average COF value. LP and aging processes show a synergistic effect in the development of hard, well-supported oxides at the interface, that enhances the frictional behavior. This is also reinforced by the friction results of INC 617-A and INC 617-A-Air, showing that the aging process alone is inadequate to provide strong surface oxides to reduce the COF.

Under ambient atmosphere (air) and at 800°C, LP-TME, and LP-TME+A, experience an initial transition zone (running-in) for 10 and 5 m, before settling to a constant state that results in average values of 0.44, and 0.47, respectively. INC 617 and LP-A depict similar COF values of 0.47 and 0.44, respectively. It can be concluded that operating under HT air environment provide sufficiently strong compact oxide to the extent that it overshadows any enhancement by LP processes. It should be, however, emphasized that INC 617 is aimed to operate under He environment.

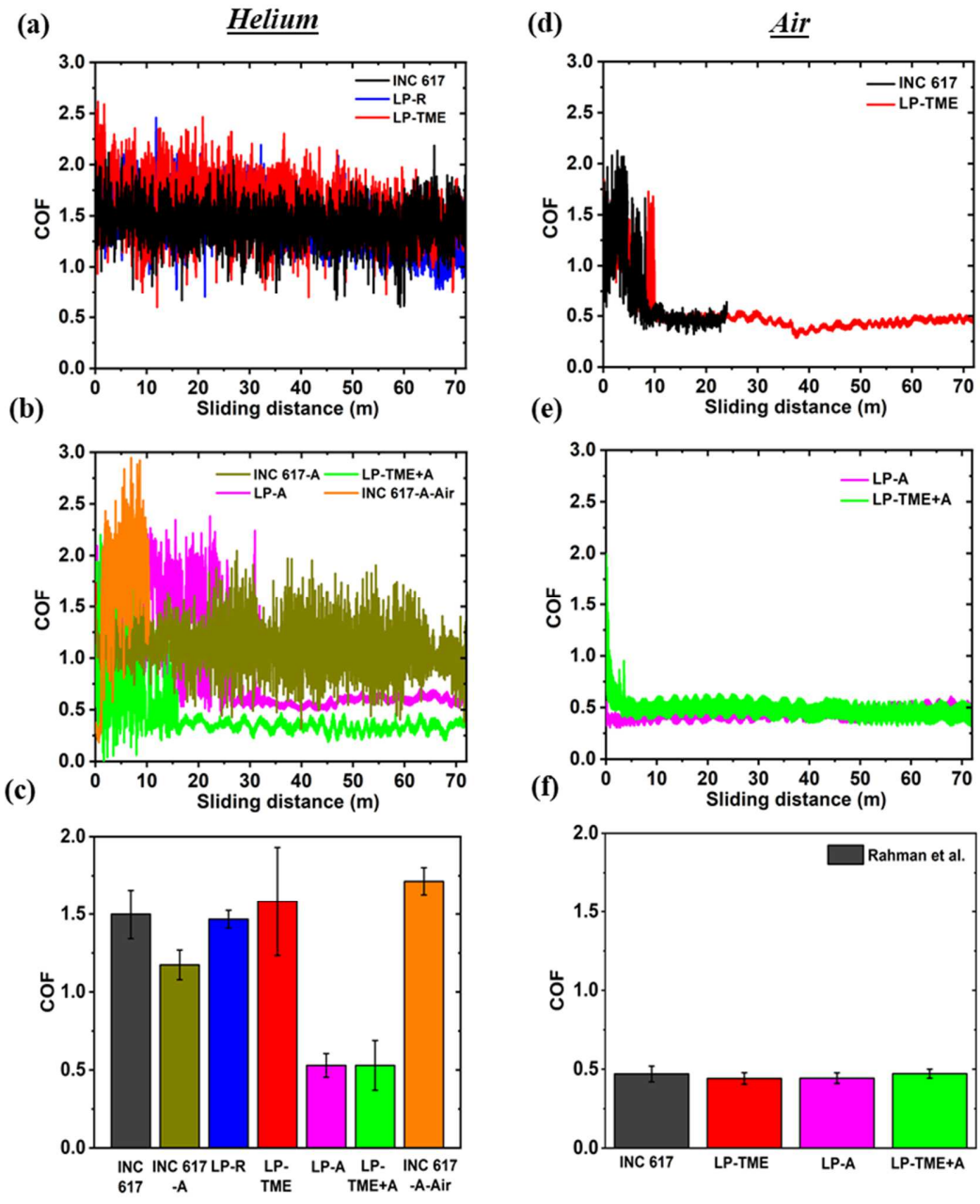

Fig. 5. *Evolution of COF with sliding distance in (a) and (b) He, and (d) and (e) air environment at 800°C, and the corresponding average values (c), and (f), respectively [18].*

Fig. 6 shows 2D and 3D profilometric scans of the worn disks following tribo-experiments under He and air environments. Both the width and the depth of the wear track give a direct measurement of the wear and severity of the contact. INC 617, INC 617-A, and LP-TME specimens appear with

a wear up to 50 µm in depth, while the penetration depth of LP-R is 80 µm. In sharp contrast, both LP aged disks, namely LP-A and LP-TME+A exhibit maximum wear depths of less than 20 µm as well as an indication of material piled ups. **Fig. 6(b)** captures the 3D topography of the disk specimens and covers both the wear tracks and unworn areas. Accumulation of loose debris is evident on the worn surface of INC 617 and INC 617-A, along with a wide wear track, similar to LP-TME, whereas LP-R appears with a deep, yet narrow wear track. In agreement with the friction data, however, LP-A and LP-TME+A feature low wear and the formation of high peaks, which are identified as compacted islands of oxides, thereafter. Similarly, the disk specimens tested under air, exhibit minute wear, and the wear tracks are mostly covered by surface oxides (see **Fig. 6(c)**). It can be postulated that regardless of the surface treatment, the disk specimens are favorable in developing an oxide tribo-layer when exposed to HT air, which results in low friction and wear, however, it is not the case in He environment where only combined LP and aging process results in stable surface oxide.

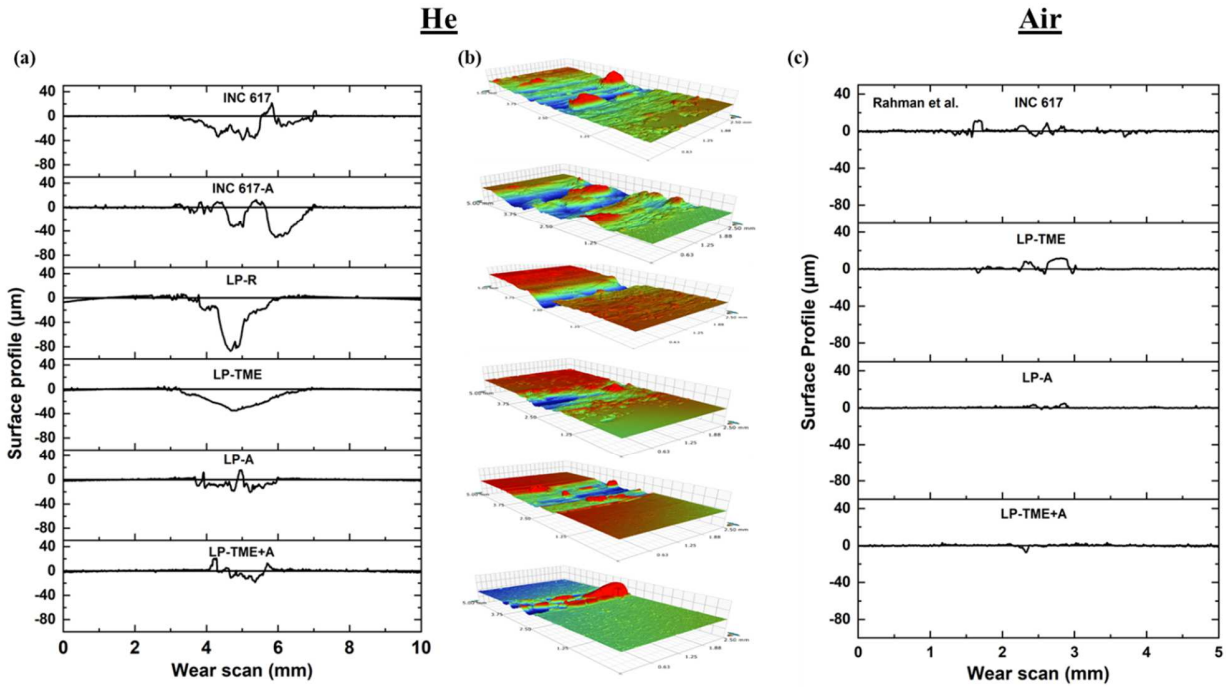

Fig. 6. *Typical (a) 2D, (b) 3D wear scans (5 × 2.5 mm area and -100 to 100 μm vertical range) of disk specimens following HT sliding in He, and (c) 2D scans after HT sliding in air.*

Fig. 7 illustrates the corresponding wear rates of the disk samples under He and air atmospheres. The worn volumes are approximated from multiple profilometric wear scans performed perpendicular to the wear track on each disk to obtain the average value, and the wear rates are calculated as described in Ref. [50]. As expected from wear track profilometry (**Fig. 6**), the LP-A and LP-TME+A samples feature the lowest amount of wear followed by INC 617-A and LP-R. INC 617 and LP-TME possess the highest wear rate values among the specimens under examination. Given the erratic nature of HT wear and the error bars, we can conclude that INC 617-A, and LP-R, INC 617 and LP-TME wear in a similar fashion. Nonetheless, significant wear reduction for aged LP and LP-TME samples is evident. Tribo-testing under air, results in negative wear rate values, as illustrated in **Fig. 7(b)** showing that oxidation overshadows material loss due to wear. The highest amount of material gain occurred on INC 617, followed by LP-TME. LP-A and LP-TME+A experience the lowest amount of surface oxidation during tribo-testing.

Figs. 7(c), and **7(d)** summarize the tribological performance of each tribo-pair under He and air, in a cumulative COF vs. wear rate plot, respectively. Under He environment, the results are scattered around low COF/low wear, high COF/high wear, and moderate regions. The experiments with INC 617, LP-R, and LP-TME fall into the high COF/high wear region with average COF values around 1.5, and a maximum wear rate of 9.42×10^{-3} mm^3/Nm, corresponding to LP-TME. However, the experiments with the LP aged specimens, namely LP-A, and LP-TME+A experience low COF/low wear values, of 0.53, 0.65, and 2.61×10^{-3}, 0.8×10^{-3} mm^3/Nm, respectively. The tribological performance of the untreated aged sample (INC 617-A) falls into the moderate region,

with an average COF value of 1.17 and wear rate at 6.8×10^{-3} mm^3/Nm, but still higher friction and wear is observed compared to LP-A, and LP-TME+A samples.

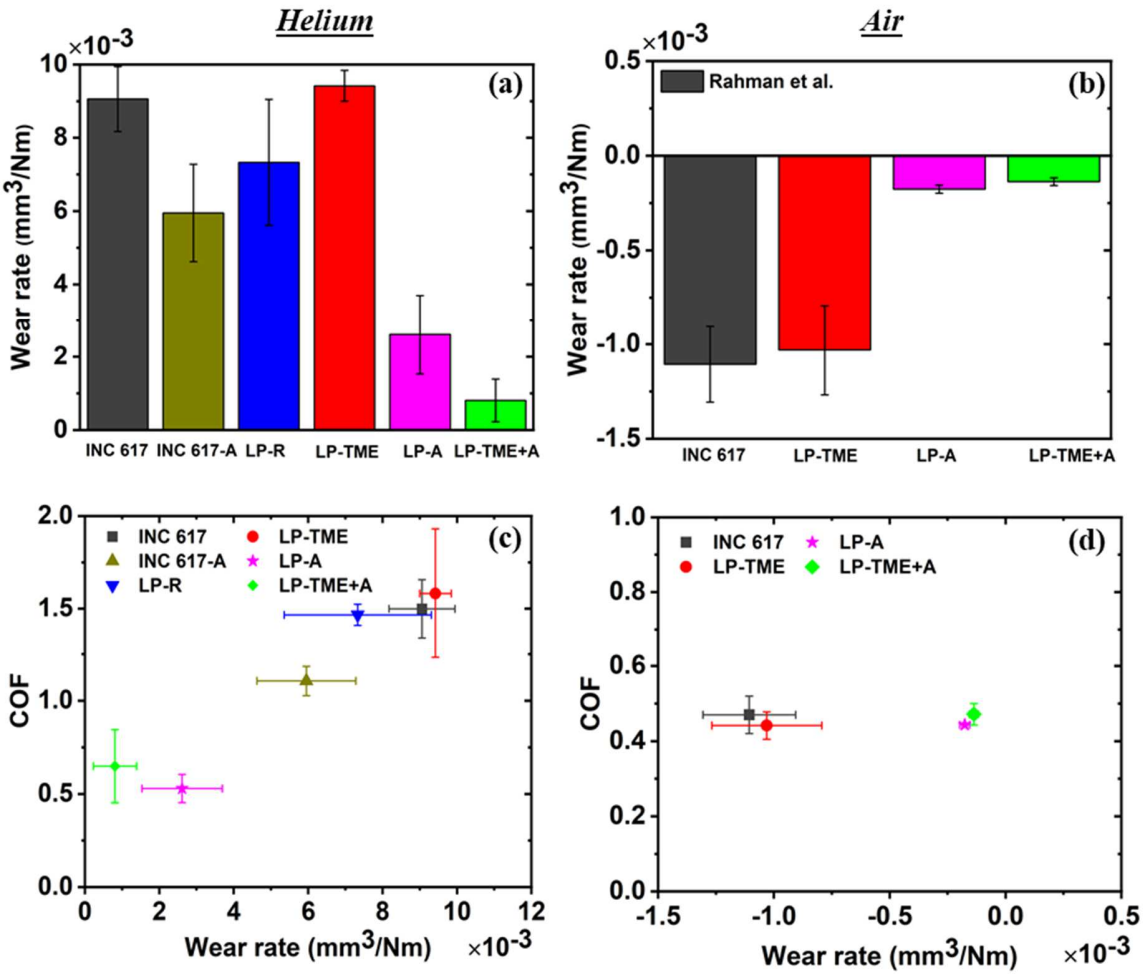

Fig. 7. *Wear rates of the disks following tribo-testing in (a) He and (b) air environment. Average COF vs. wear graphs after tribo-testing in (c) He and (d) air environment.*

3.4 Surface morphology

3.4.1 He environment

SEM micrographs of the unworn and worn surfaces of the disks after tribo-experiments in He are shown in **Fig. 8**. The orange arrows on the images of the worn areas shown on the right-hand side indicate the sliding direction of the counter surface. The left-hand side of **Fig. 8** presents the

morphology of the surface oxides developed on the matrix of the untreated and treated INC 617 disks following tribo-testing in 800°C He environment. The magnified images are shown on the sides of Fig. 8. **Table 3** details the elemental composition of the surface of both the unworn and worn regions of most of the disk specimens under examination.

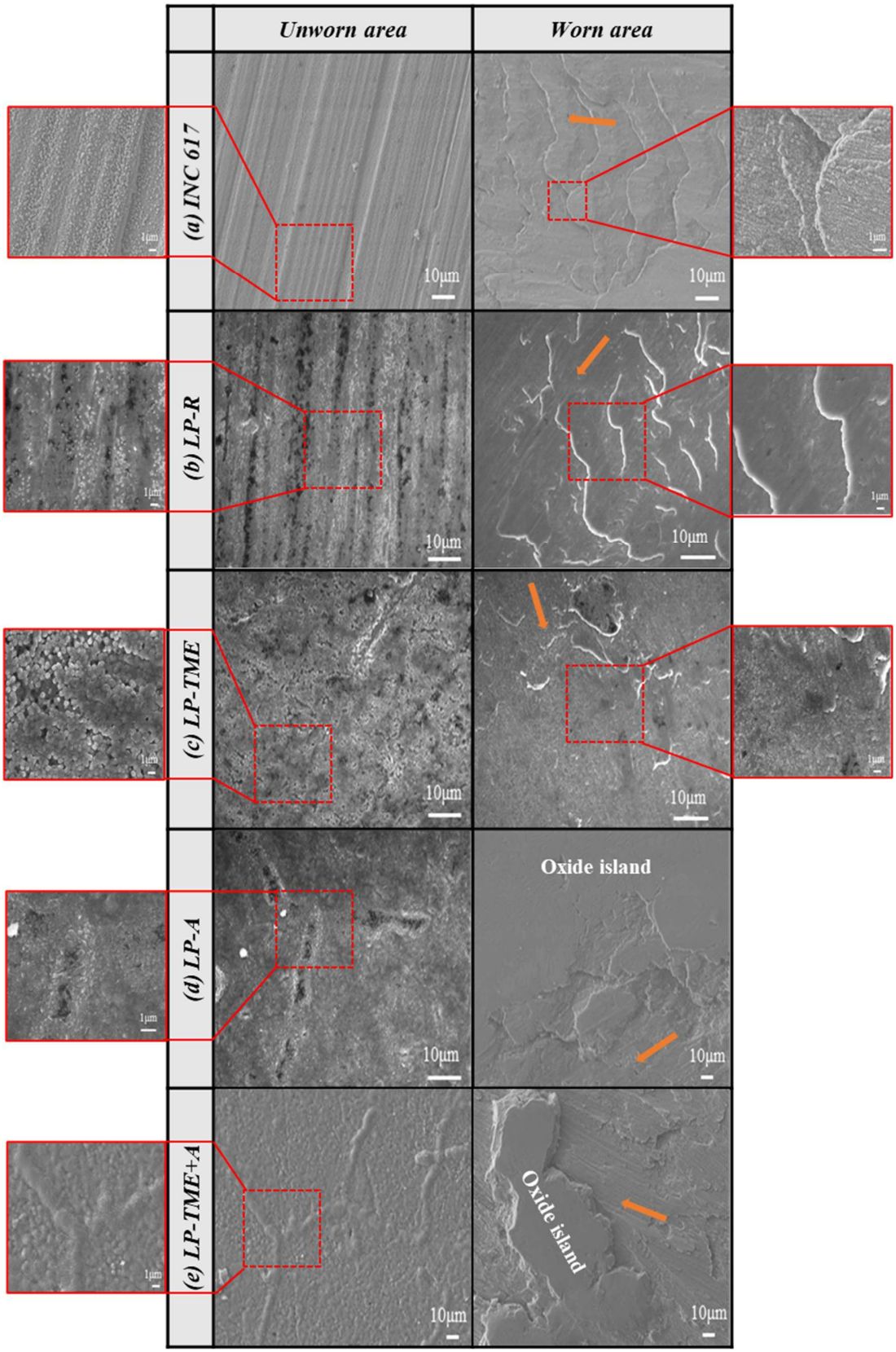
Unworn area
Worn area
(a) INC 617
(b) LP-R
(c) LP-TME
(d) LP-A
(e) LP-TME+A
Oxide island
Oxide island
10μm
1μm

Fig. 8. *SEM images of the unworn and worn surfaces of (a) INC 617, (b) LP-R, (c) LP-TME, (d) LP-A, and (e) LP-TME+A after the tribological experiments in He. Magnified images are shown on the sides of the figure. Orange arrows represent the sliding direction of the counter surface.*

Table 3*. Surface EDS on matrix and worn areas of INC 617, LP-R, LP-TME, LP-A, and LP-TME+A disk specimens following tribo-experiment in He.*

	Elements (at%)	**O**	**Al**	**Ti**	**Cr**	**Fe**	**Co**	**Ni**	**Mo**
Unworn area	INC 617	50.39	2.74	0.3	14.44	0.76	5.28	23.21	2.89
	LP-R	45.07	3.08	0.42	15.19	0.95	5.91	25.8	3.6
	LP-TME	49.47	2.1	0.53	14.83	0.78	5.29	24.25	2.75
	LP-A	71.17	0.32	0.79	26.66	0.24	0.2	0.55	0.07
	LP-TME+A	66.05	0.2	1.01	30.3	0.26	0.31	1.64	0.23
Worn area	INC 617	43.23	1.88	0.24	15.47	0.88	6.38	28.7	3.23
	LP-R	25.8	1.72	0.4	18.85	1.56	8.61	39.28	4.28
	LP-TME	35.78	1.83	0.34	16.27	1.12	7.46	33.49	3.71
	LP-A	59.51	0.68	0.31	13.61	0.74	4.68	18.58	1.89
	LP-TME+A	66.51	0.97	0.31	16.03	0.55	2.92	11.68	1.03

Despite the minute presence of oxygen-containing groups (O_2, H_2O, CO, CO_2) within the testing chamber and the aging furnace, it is sufficient to promote the formation of different types of superficial metal oxides on all specimens as reported in Refs. [15,17,18]. Note that the HT tribo-testing for 30 minutes at 800°C in He, can be considered as a short-time aging process, during which fast oxidation kinetics encourage the reactivity of surface atoms with the surrounding atmosphere. The INC 617 matrix appears full of uniformly distributed surface oxide particles. The unworn surface of LP-R shows similar surface oxide particles, as INC 617, with a diameter of less than 500 nm, but finer oxides are also observed in between (gray regions), thus the overall surface

oxidation is reduced by the LP process, as also supported by previous studies (e.g., see Ref. [51]). The virgin area of LP-TME appears with larger oxides of around 1 μm in diameter and with a marginal increased percentage of surface oxidation, compared to LP-R. Furthermore, the unworn surface of the aged specimens, namely LP-A, and LP-TME+A feature homogeneous distribution of nodular-like oxides, where several oxides are merged forming long and continuous ridges along the grain boundaries (indicated with white arrows). Comparing the elemental composition of the LP aged specimens (LP-A, LP-TME+A) with the unaged ones (LP-R, LP-TME) of **Table 3**, it can be inferred that the surface of the specimens that underwent aging process was mainly covered by Cr-oxide, whereas a Ni-Cr-O mixed oxide layer appears on the unaged specimens. Also, the amount of O found on LP-A, and LP-TME+A specimens is significantly higher than the amount of the unaged ones due to adequate surface oxidation that was promoted during the aging process.

Investigating the morphology of the worn areas allows correlations with the frictional and wear performance of the tribo-pairs. INC 617, LP-R, and LP-TME, depict similar wear modes, namely oxidative adhesion, and delamination. Deformed surface oxides are evident on the wear tracks of both specimens, without any indication of agglomeration. LP-R features the smallest amount of oxide particles, in accord with the quantitative analysis shown in **Table 3**. On the other hand, compacted oxide tribo-layers are found on the wear tracks of the aged samples (LP-A, LP-TME+A), and are identified as Ni-Cr-O mixed oxides. The accumulation and compaction of surface oxide particles result in a significantly higher amount of oxygen in these regions, which are characterized as islands of oxides. Such thick glazed oxides that evidently are further stabilized by the LP process provide an excellent protective layer with lubricating characteristics that results in low COF and wear [2,5]. Furthermore, the running-in period of the aged tribo-pairs, seen in **Fig. 5(a),** describes the time needed for the compacted glazed oxides to be generated, until a constant

zone is reached. In fact, some of the surface oxides are removed from the interface as loose debris, but more importantly some others undergone a shearing, compaction, and accumulation, and thus developing stabilized and strong oxide layers and islands. Longer running-in time for LP-A than LP-TME+A, indicates that more surface material was purged out, until compacted oxide layers were generated. Therefore, the wear rate of LP-A is higher than LP-TME+A as shown in **Fig. 7**.

The pre-oxidation (aging) process contributes to the subsequent development of compacted surface oxides within the contact region during sliding, which results in enhanced tribological performance. As discussed, experiments following LP, LP+TME, and post aging processes were performed (e.g., see **Fig. 5)** in an effort to further understand the contribution of each surface and thermal treatments on the tribological response of the tribo-pairs. A synergistic effect of the two surface treatment techniques, namely LP, and aging takes place herein, and eventually strong, well-supported compacted oxide layers are formed during sliding, significantly mitigating friction and wear (LP-A, LP-TME+A). The aging process by itself does not result in measurable tribological enhancements as poor tribological performance is observed for tribo-pair INC 617-A. Also, in a similar study on untreated aged alloy 800HT, high friction and wear values were observed due to the inadequateness of strong, well-supported oxides to be sustained at the interface [44]. It can be hypothesized that the load bearing capability of the subsurface is poor, due to thermal softening at HT, and the plastic deformation of the untreated subsurface induces delamination and removal of the surface oxides [52].

Herein, the LP process induces compressive residual stresses, plastic deformation, defects, and fine grains, resulting in an enhanced surface/subsurface structure, which is retained even after aging the specimens at 950°C (LP-A, LP-TME+A), as seen in **Fig. 3**. As the LP process alleviates

a degree of thermal softening of the subsurface, it is able to support the integrity of the superficial oxide tribo-layers, which provide low friction and wear [43]. Another influencing mechanism could be a stronger interfacial bond between the oxide and substrate promoted by the strengthening effect of the LP process. Interfacial bond improvement is also reported by Kanjer et al. and Lavisse et al [20-22] for titanium alloys. They concluded that LP could enhance the adherence of surface oxides by the formation of an intermediate nitride layer on titanium and titanium-based substrates following thermal aging (oxidation) in air environment. While interfacial bond improvement can also be a contributing factor, intermediate nitride layer formation cannot be concluded as the aging process and the tribological tests were all carried out in an impure (99.999%) He environment. The chemical composition of the sample also does not show significant amount of N. Rather, here, the stronger interfacial bond is attributed to the microstructural improvements by LP process. In addition to LP process itself, the aging provides the surface with adequate pre-oxidation (**Table 3**), in which during sliding surface oxide layers and bulky oxide islands are formed, supported by the LP treated subsurface. Therefore, low COF and wear values are observed. Also, the wear resistance of the LP subsurface is enhanced [30,31,34] and the hard oxide particles are more likely to remain at the interface and form oxide layers, instead of plowing on the contacting surface.

3.4.2 Air environment

The same tribo-testing was repeated for the LP tribo-pairs by changing the environment to ambient air, so the effect of the atmosphere on the tribological performance can be further explored. **Fig. 9** shows microscopic images of the worn regions of LP-TME, LP-A, and LP-TME+A disk and pin specimens, following sliding in air environment. It is apparent that surface oxides are respectively generated along the wear tracks and the wear scars of all disks and pins resulting in low COF and wear values. LP-TME (**Fig. 9(a)**) demonstrates well-developed and more compacted oxide layers,

compared to LP-A (**Fig. 9(b)**), and LP-TME+A (**Fig. 9c**)) disks. This is in accord with the longer running-in time of the former, whereas LP-A, and LP-TME+A appear with almost a constant COF from the beginning of the experiment, as shown in **Fig. 5(b)**. Also, the wear scars of all pins appear to be mostly covered by a thick oxide layer. Several studies were carried out investigating the tribological behavior of metal alloys sliding in HT open environment. It is widely understood that the tribological performance is mainly driven by the oxidation of the rubbing surfaces, that is inevitably taking place in ambient air at HT [53]. In fact, the open environment gives a plethora of oxygen-containing sites that during sliding, tribo-chemical interactions are taking place at the interface, and new fresh oxides are formed continuously replacing the worn ones [17]. This is more pronounced during HT sliding in air, since in He the concentration of O-containing groups in the surrounding atmosphere is significantly lower, and tribo-chemical interactions are much slower, which hinders the formation of new oxides. This is also in line with the wear rate results shown in **Fig. 7(b)**, wherein significant surface oxidation resulted in "negative wear," or material gain in all disk specimens tested in ambient environment. As stated earlier, regardless of the surface modifications and post-aging processes on INC 617, enhanced tribological characteristics prevail in HT air, attributed to different surface oxides, mainly Cr_2O_3 [15,17,18].

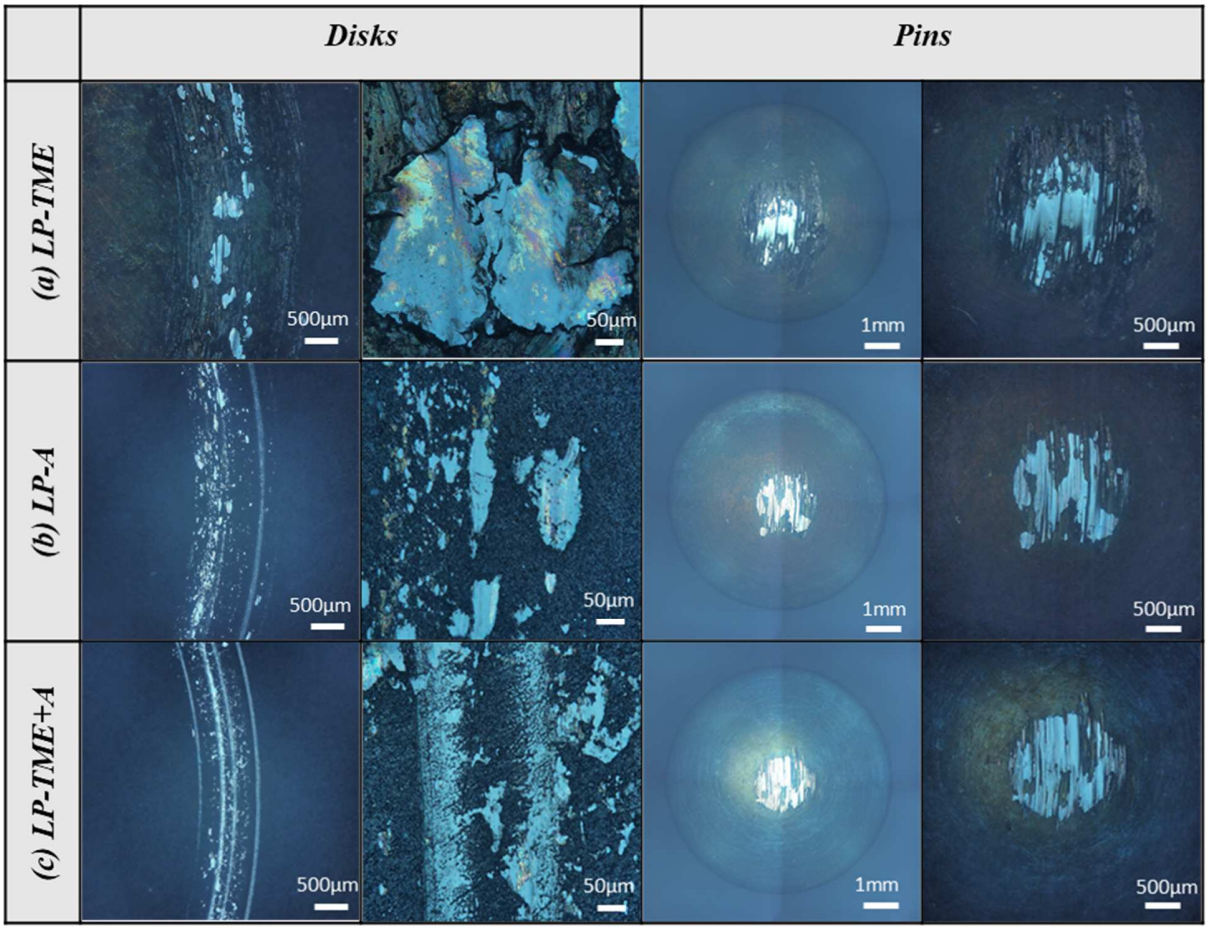

Fig. 9. *Optical microscopic images of the worn disks and pins of (a) LP-TME, (b) LP-A, and (c) LP-TME+A after sliding in air.*

3.5 *Elemental analysis – Cross section EDS*

Fig. 10 presents the cross-section EDS mapping of the unworn areas of the LP disk specimens, namely LP-R, LP-TME, LP-A, and LP-TME+A after the tribo-experiments in He atmosphere. **Fig. 10(a)** depicts that the main elements were evenly distributed along the thickness of LP-R. The cross-section EDS mapping of LP-TME shows higher surface and subsurface oxidation with a partition of Cr, and Al respectively (**Fig. 10(b)**). On the contrary, both aged samples, namely LP-A, and LP-TME+A appear with a superficial dense oxide layer of thickness around 6, and 3 µm, as shown in **Figs. 10(c)**, and **(d)**, respectively. The thickness of the surface oxide also shows that

our microhardness test depth was sufficient to penetrate deep into the materials reducing oxide effects. **Figs. 10(c)**, and **(d)** reveal the surface oxides to be predominantly Cr-oxides with a partition of Mn, and the presence of subsurface oxides of Al. Cr-rich surface oxides are formed on the surface of INC 617 during HT aging in He atmosphere [2,4,15,17,18]. Rahman et. al. investigated the surface of INC 617 aged in He for 100 hours via XRD, and identified the surface oxides to be mainly composed of Cr_2O_3, and $(Ni/Mn)Cr_2O_4$ [17]. Also, Al is found below the surface oxide suggesting that O is diffused into the matrix and reacts with Al, as also reported in Refs. [2,17,18].

Fig. 11 maps the elements found on the cross-section of the worn regions of the disk specimens following tribo-sliding under He atmosphere. The topmost layers of LP-R had a marginal increase in the amount of O, and the main elements are evenly distributed within the subsurface, as shown in **Fig. 11(a)**. **Fig. 11(b)** demonstrates that LP-TME experiences a higher concentration of O at the topmost layer, where a uniform oxide layer is observed. The amount of surface oxidation on LP-R, and LP-TME disk specimens is not adequate to promote the development of compacted oxide glazes at the interface, hence, a high COF and wear values are observed. On the other hand, the worn area of LP-A appears with a Cr-rich oxide layer, around 6 μm thick with an apparent subsurface Al oxidation, as shown in **Fig. 11(c)**.

During HT sliding, the pre-formed surface oxide particles are merged under pressure by compaction and maintained on the surface. More importantly, the superficial oxides, supported by the LP subsurface, develop bulky islands of oxides, of 40 μm thick (**Fig. 6(b)**), which provided excellent lubrication at the interface with low COF and wear values. To further examine the strengthening effect of the islands of compacted oxides, Vickers microhardness measurements were taken targeting selected areas. The microhardness results ranged from 3.5 to 7.5 GPa, with a

corresponding penetration depth of 6.3 to 3.4 μm. Such high hardness makes them highly durable during sliding, terminating further wear and maintaining low COF. Similarly, LP-TME+A appeared with mainly Cr-oxide on the surface and Al-oxide underneath. Again, islands of oxides up to 80 μm thick formed at the sliding interface, and efficiently separated the 2 metallic surfaces where a favorable tribological response was observed. The microhardness values ranged from 3.7 to 7.8 GPa, with maximum indentation depths of 5.5 and 3.8 μm, respectively.

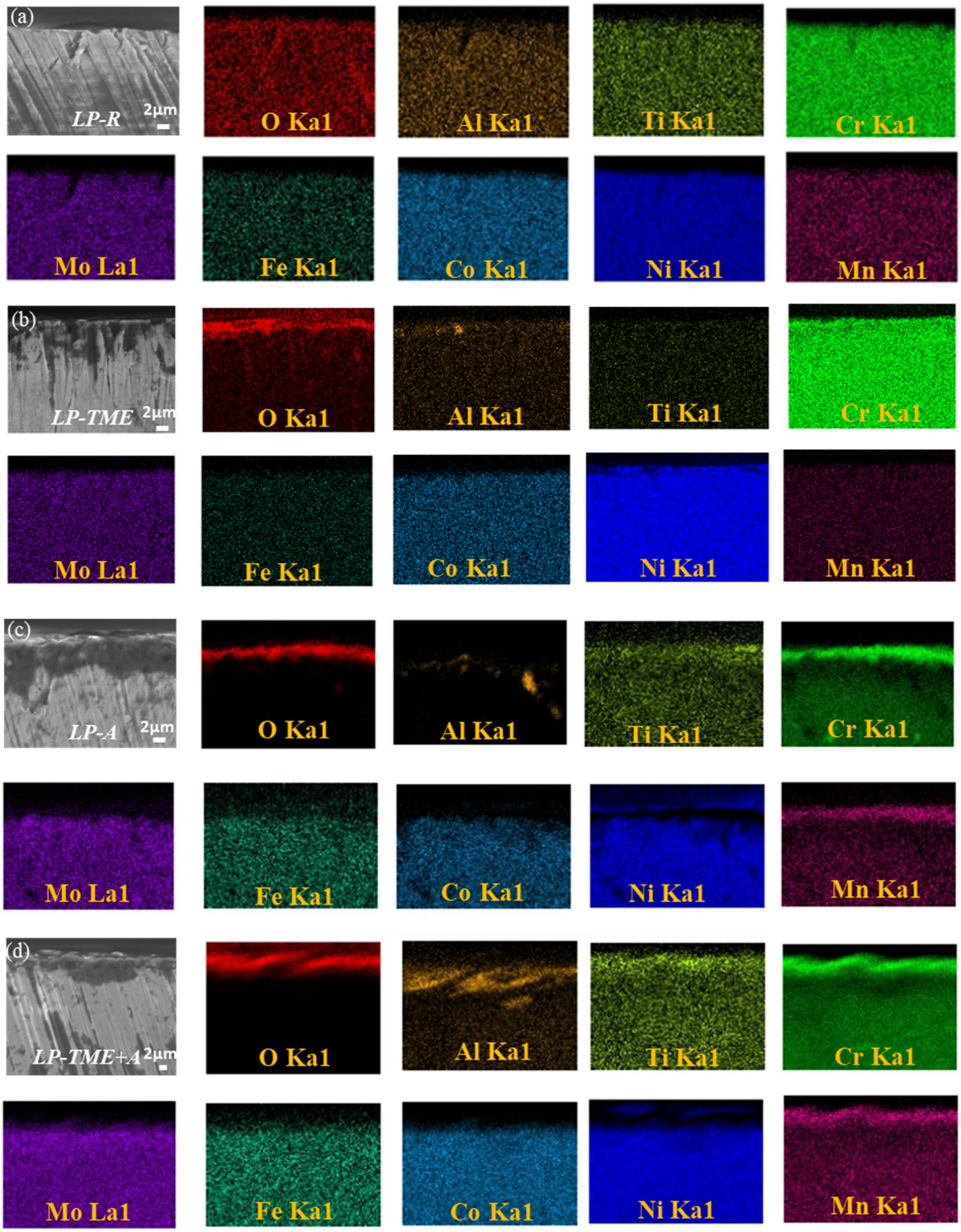

Fig. 10. *Cross-section SEM images and EDS maps of the unworn areas (matrix) after HT tribo-testing in He of (a) LP-R, (b) LP-TME, (c) LP-A, and (d) LP-TME+A.*

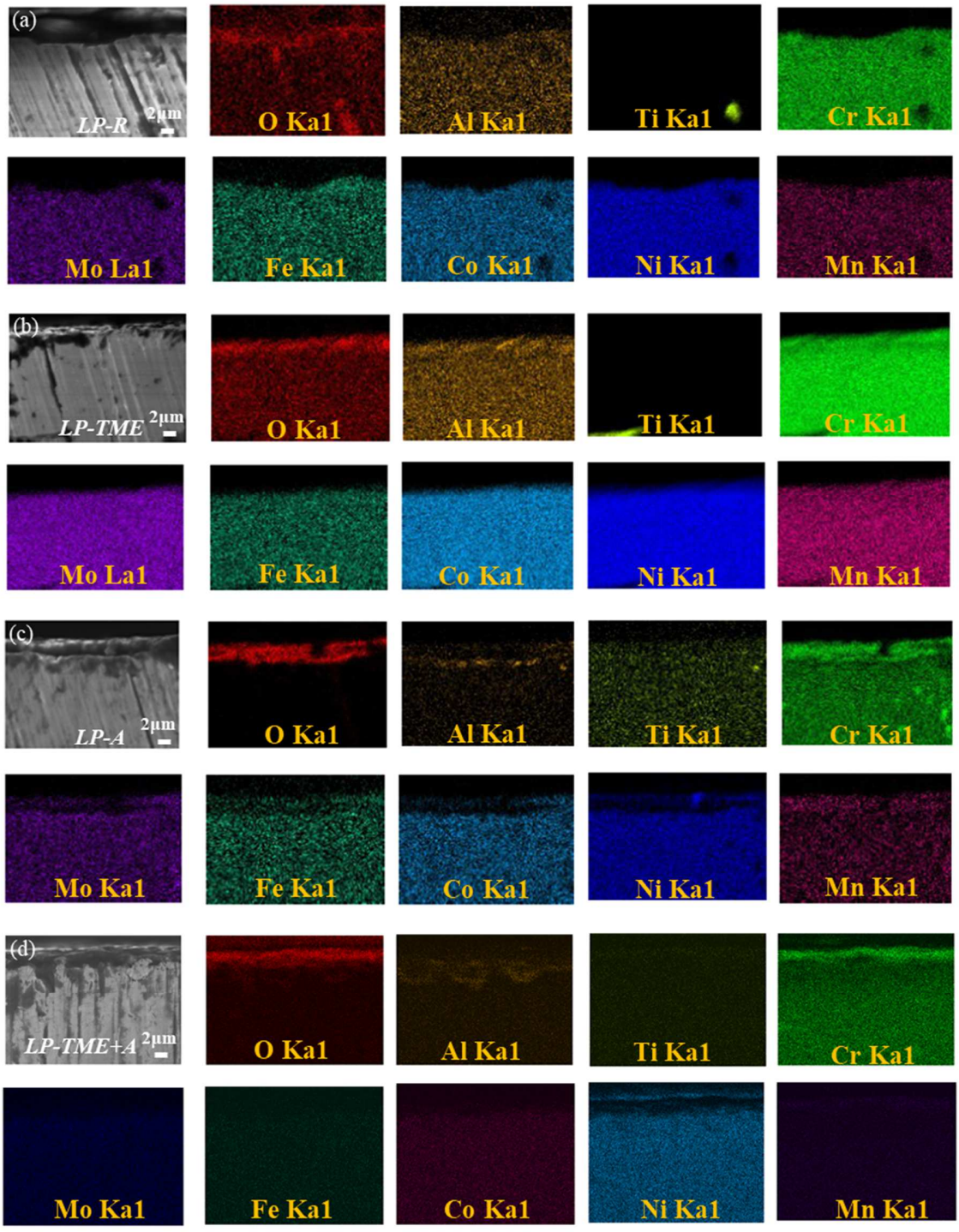

Fig. 11*. Cross-section SEM images and EDS maps of the worn areas after HT tribo-testing in He of (a) LP-R, (b) LP-TME, (c) LP-A, and (d) LP-TME+A.*

4. Conclusion

This study investigated the effect of surface modifications, namely LP, TME and post-treatment aging on the tribological performance of INC 617 in HTGR/VHTR (He) and air environments. The following conclusions can be drawn:

- The LP process, itself increases the surface microhardness by 62%, whereas the TME process adds a marginal increase on the average microhardness, due to the additional effect of precipitation hardening. After the aging process (950°C-10 hours) relaxation and annihilation of the LP-induced stresses and microstructure are prevented, as evident by relatively preserved hardness values. This is also supported by the stabilized microstructure captured through TEM imaging after 60 hours of thermal exposure.
- LP-A and LP-TME+A depicted excellent tribological behavior under impure He environment due to the high amount of pre-oxidation and the supportive role of the LP surface and subsurface to stabilized surface oxides, in contrast with INC 617-A.
- Tribo-testing in HT air environment diminished the effect of surface modifications since adequate continuous surface oxidation at the sliding interface results in low friction and wear overshadowing any other enhancement, if any.
- The findings of this work show that a post-treatment aging process can be coupled with a pre-treatment LP process on the HT superalloy, namely INC 617 to enhance the tribo-response of mechanical components in HT He applications (i.e., VHTR/HTGR). However, the underlying mechanism involved in the process needs to be comprehensively studied in future works to enhance and optimize the process and to pave the way for effective commercialization of the LP process for HT nuclear reactor components under tribological and potentially tribo-corrosive environments.

Acknowledgments

This research work was motivated in part by the U.S. Department of Energy (DOE) under Nuclear Energy University Program (NEUP) Project 16-10732. The authors would like to thank Dr. Richard Wright of Idaho National Lab (INL) for providing samples and valuable information. The authors also acknowledge the use of the Texas A&M Materials Characterization Facility (MCF), where SEM, and EDS experiments were performed. Keivan Davami extends gratitude to the Alabama Transportation Institute (ATI) for their support of this research. Keivan Davami also acknowledges the support of the Advanced Manufacturing program of the National Science Foundation, award CMMI-AM #2029059.

References

[1] J. Gentzbittel, High temperature corrosion of structural materials under gas-cooled reactor helium, (2006). https://doi.org/10.1002/maco.200503901.

[2] V. Pauly, J. Kern, M. Clark, D.S. Grierson, K. Sridharan, Tribology International Wear Performance of incoloy 800HT and inconel 617 in various surface conditions for high-temperature gas-cooled reactor components, Tribol. Int. 154 (2021) 106715. https://doi.org/10.1016/j.triboint.2020.106715.

[3] R.N. Wright, R.N. Wright, Summary of Studies of Aging and Environmental Effects on Inconel 617 and Haynes 230 Effects on Inconel 617 and Haynes 230, (n.d.).

[4] V. Pauly, C. Tesch, J. Kern, M. Clark, D. Grierson, D. Singh, O. Ajayi, K. Sridharan, High-temperature tribological behavior of structural materials after conditioning in impure-helium environments for high-temperature gas-cooled reactor applications, J. Nucl. Mater. 522 (2019) 311–323. https://doi.org/10.1016/j.jnucmat.2019.05.025.

[5] W. Sun, A.W. Tan, D. Jia, Y. King, N. Win, A. Bhowmik, Surface & Coatings Technology Tribological behavior of cold sprayed Inconel 718 coatings at room and elevated temperatures, Surf. Coat. Technol. 385 (2020) 125386. https://doi.org/10.1016/j.surfcoat.2020.125386.

[6] M. Fulger, D. Ohai, M. Mihalache, M. Pantiru, V. Malinovschi, Oxidation behavior of Incoloy 800 under simulated supercritical water conditions, J. Nucl. Mater. 385 (2009) 288–293. https://doi.org/10.1016/j.jnucmat.2008.12.004.

[7] H. Akhiani, M. Nezakat, S. Penttilä, J. Szpunar, The Journal of Supercritical Fluids The oxidation resistance of thermo-mechanically processed Incoloy 800HT in supercritical water, J. Supercrit. Fluids. 101 (2015) 150–160. https://doi.org/10.1016/j.supflu.2015.03.019.

[8] G.A. El-awadi, S. Abdel-samad, E.S. Elshazly, Applied Surface Science Hot corrosion behavior of

Ni based Inconel 617 and Inconel 738 superalloys, Appl. Surf. Sci. 378 (2016) 224–230. https://doi.org/10.1016/j.apsusc.2016.03.181.

[9] D. Saber, I.S. Emam, R. Abdel-karim, High temperature cyclic oxidation of Ni based superalloys at different temperatures in air, J. Alloys Compd. 719 (2017) 133–141. https://doi.org/10.1016/j.jallcom.2017.05.130.

[10] W. Osthoff, H. Schuster, P.J. Ennis, H. Nickel, Creep and Relaxation Behavior of Inconel-617., Nucl. Technol. 66 (1984) 296–307. https://doi.org/10.13182/NT84-A33433.

[11] Y. Birol, Thermal fatigue testing of Inconel 617 and Stellite 6 alloys as potential tooling materials for thixoforming of steels, Mater. Sci. Eng. A. 527 (2010) 1938–1945. https://doi.org/10.1016/j.msea.2009.11.021.

[12] W.L. Mankins, J.C. Hosier, T.H. Bassford, Microstructure and Phase Stability of Inconel Alloy 617., Met. Trans. 5 (1974) 2579–2590. https://doi.org/10.1007/BF02643879.

[13] S. Salari, M.S. Rahman, A.A. Polycarpou, A. Beheshti, Elevated temperature mechanical properties of Inconel 617 surface oxide using nanoindentation, Mater. Sci. Eng. A. 788 (2020) 139539. https://doi.org/10.1016/j.msea.2020.139539.

[14] S. Salari, A. Beheshti, Asperity-based contact and static friction with provision for creep: A review, Surfaces and Interfaces. 24 (2021). https://doi.org/10.1016/j.surfin.2021.101144.

[15] M.S. Rahman, J. Ding, A. Beheshti, X. Zhang, A.A. Polycarpou, Elevated temperature tribology of Ni alloys under helium environment for nuclear reactor applications, Tribol. Int. 123 (2018) 372–384. https://doi.org/10.1016/j.triboint.2018.03.021.

[16] A. Ahmadi, F. Sadeghi, S. Shaffer, In-situ friction and fretting wear measurements of Inconel 617 at elevated temperatures, Wear. 410–411 (2018) 110–118. https://doi.org/10.1016/j.wear.2018.06.007.

[17] M.S. Rahman, K. Polychronopoulou, A.A. Polycarpou, Tribochemistry of inconel 617 during sliding contact at 950 °C under helium environment for nuclear reactors, J. Nucl. Mater. 521 (2019) 21–30. https://doi.org/10.1016/j.jnucmat.2019.04.032.

[18] M.S. Rahman, J. Ding, A. Beheshti, X. Zhang, A.A. Polycarpou, Helium Tribology of Inconel 617 at Elevated Temperatures up to 950°C: Parametric Study, Nucl. Sci. Eng. 193 (2019) 998–1012. https://doi.org/10.1080/00295639.2019.1582315.

[19] Y. Zhang, D.P. Mohanty, P. Seiler, T. Siegmund, J.J. Kruzic, V. Tomar, High temperature indentation based property measurements of IN-617, Int. J. Plast. 96 (2017) 264–281. https://doi.org/10.1016/j.ijplas.2017.05.007.

[20] A. Kanjer, L. Lavisse, V. Optasanu, P. Berger, C. Gorny, P. Peyre, F. Herbst, O. Heintz, N. Geoffroy, T. Montesin, M.C.M. De Lucas, Surface & Coatings Technology Effect of laser shock peening on the high temperature oxidation resistance of titanium, Surf. Coat. Technol. 326 (2017) 146–155. https://doi.org/10.1016/j.surfcoat.2017.07.042.

[21] L. Lavisse, A. Kanjer, P. Berger, V. Optasanu, C. Gorny, P. Peyre, T. Montesin, M.C.M. De Lucas, Surface & Coatings Technology High temperature oxidation resistance and microstructure of laser-shock peened Ti-Beta-21S, Surf. Coat. Technol. 403 (2020) 126368. https://doi.org/10.1016/j.surfcoat.2020.126368.

[22] A. Kanjer, V. Optasanu, L. Lavisse, Influence of Mechanical Surface Treatment on High-Temperature Oxidation of Pure Titanium, (2017) 383–395. https://doi.org/10.1007/s11085-016-

9700-6.

[23] A.S. Gill, A. Telang, V.K. Vasudevan, Journal of Materials Processing Technology, Characteristics of surface layers formed on inconel 718 by laser shock peening with and without a protective coating, 225 (2015) 463–472. https://doi.org/10.1016/j.jmatprotec.2015.06.026.

[24] J. Kusin, M. Rozmus-go, Effect of Laser Shock Peening on the Microstructure and Properties of the Inconel 625 Surface Layer, 29 (2020) 1544–1549. https://doi.org/10.1007/s11665-020-04667-3.

[25] M. Munther, T. Martin, A. Tajyar, L. Hackel, A. Beheshti, K. Davami, Laser shock peening and its effects on microstructure and properties of additively manufactured metal alloys: A review, Eng. Res. Express. 2 (2020) 22001. https://doi.org/10.1088/2631-8695/ab9b16.

[26] A.S. Gill, A. Telang, C. Ye, S.R. Mannava, D. Qian, V.K. Vasudevan, Materials Characterization Localized plastic deformation and hardening in laser shock peened Inconel alloy 718SPF, Mater. Charact. 142 (2018) 15–26. https://doi.org/10.1016/j.matchar.2018.05.010.

[27] D. Karthik, S. Swaroop, Laser shock peening enhanced corrosion properties in a nickel based Inconel 600 superalloy, J. Alloys Compd. 694 (2017) 1309–1319. https://doi.org/10.1016/j.jallcom.2016.10.093.

[28] J. Sheng, H. Zhang, X. Hu, S. Huang, Influence of laser peening on the high-temperature fatigue life and fracture of Inconel 718 nickel-based alloy, Theor. Appl. Fract. Mech. 109 (2020) 102757. https://doi.org/10.1016/j.tafmec.2020.102757.

[29] U. Trdan, M. Skarba, J.A. Porro, J.L. Ocaña, J. Grum, Application of massive laser shock processing for improvement of mechanical and tribological properties, Surf. Coatings Technol. 342 (2018) 1–11. https://doi.org/10.1016/j.surfcoat.2018.02.084.

[30] Y. Guo, S. Wang, W. Liu, Z. Sun, G. Zhu, T. Xiao, Effect of laser shock peening on tribological properties of magnesium alloy ZK60, Tribol. Int. 144 (2020). https://doi.org/10.1016/j.triboint.2019.106138.

[31] J. Zhou, Y. Sun, S. Huang, J. Sheng, J. Li, E. Agyenim-Boateng, Effect of laser peening on friction and wear behavior of medical Ti6Al4V alloy, Opt. Laser Technol. 109 (2019) 263–269. https://doi.org/10.1016/j.optlastec.2018.08.005.

[32] I. Yakimets, C. Richard, G. Béranger, P. Peyre, Laser peening processing effect on mechanical and tribological properties of rolling steel 100Cr6, Wear. 256 (2004) 311–320. https://doi.org/10.1016/S0043-1648(03)00405-8.

[33] D. Kumar, S. Nadeem Akhtar, A. Kumar Patel, J. Ramkumar, K. Balani, Tribological performance of laser peened Ti-6Al-4V, Wear. 322–323 (2015) 203–217. https://doi.org/10.1016/j.wear.2014.11.016.

[34] A. Siddaiah, B. Mao, Y. Liao, P.L. Menezes, Surface characterization and tribological performance of laser shock peened steel surfaces, Surf. Coatings Technol. 351 (2018) 188–197. https://doi.org/10.1016/j.surfcoat.2018.07.087.

[35] S.A. Kumar, R. Sundar, S.G.S. Raman, Effects of laser peening on fretting wear behaviour of alloy 718 fretted against two different counterbody materials, 231 (2017) 1276–1288. https://doi.org/10.1177/1350650117692707.

[36] A.N. Jinoop, S.K. Subbu, C.P. Paul, I.A. Palani, Post-processing of Laser Additive Manufactured Inconel 718 Using Laser Shock Peening, International Journal of Precision Engineering and

Manufacturing, 20 (2019) 1621–1628. https://doi.org/10.1007/s12541-019-00147-4.

[37] M. Munther, R.A. Rowe, M. Sharma, L. Hackel, K. Davami, Thermal stabilization of additively manufactured superalloys through defect engineering and precipitate interactions, Mater. Sci. Eng. A. 798 (2020) 140119. https://doi.org/10.1016/j.msea.2020.140119.

[38] W. Cao, M. Khadhraoui, B. Brenier, J.Y. Guédou, L. Castex, Thermomechanical relaxation of residual stress in shot peened nickel base superalloy, Mater. Sci. Technol. (United Kingdom). 10 (1994) 947–954. https://doi.org/10.1179/mst.1994.10.11.947.

[39] Y. Li, L. Zhou, W. He, G. He, X. Wang, X. Nie, B. Wang, S. Luo, Y. Li, The strengthening mechanism of a nickel-based alloy after laser shock processing at high temperatures, Sci. Technol. Adv. Mater. 14 (2013). https://doi.org/10.1088/1468-6996/14/5/055010.

[40] Z. Zhou, A.S. Gill, A. Telang, S.R. Mannava, K. Langer, V.K. Vasudevan, D. Qian, Experimental and Finite Element Simulation Study of Thermal Relaxation of Residual Stresses in Laser Shock Peened IN718 SPF Superalloy, Exp. Mech. 54 (2014) 1597–1611. https://doi.org/10.1007/s11340-014-9940-9.

[41] M. Kattoura, S.R. Mannava, D. Qian, V.K. Vasudevan, Effect of laser shock peening on residual stress, microstructure and fatigue behavior of ATI 718Plus alloy, Int. J. Fatigue. 102 (2017) 121–134. https://doi.org/10.1016/j.ijfatigue.2017.04.016.

[42] T. Palma, M. Munther, M. Sharma, L. Hackel, A. Beheshti, K. Davami, Nanomechanical Characterization of Laser Peened Additively Manufactured Inconel 718 Superalloy, Adv. Eng. Mater. 21 (2019) 1–9. https://doi.org/10.1002/adem.201900499.

[43] Z.P. Tong, X.D. Ren, W.F. Zhou, S. Adu-Gyamfi, L. Chen, Y.X. Ye, Y.P. Ren, F.Z. Dai, J.D. Yang, L. Li, Effect of laser shock peening on wear behaviors of TC11 alloy at elevated temperature, Opt. Laser Technol. 109 (2019) 139–148. https://doi.org/10.1016/j.optlastec.2018.07.070.

[44] M.S. Rahman, K. Polychronopoulou, A.A. Polycarpou, Tribochemical changes of alloy 800HT under sliding contact at elevated temperature in impure helium environment, Wear. 462–463 (2020). https://doi.org/10.1016/j.wear.2020.203508.

[45] A.M. Mostafa, M.F. Hameed, S.S. Obayya, Effect of laser shock peening on the hardness of AL-7075 alloy, J. King Saud Univ. - Sci. 31 (2019) 472–478. https://doi.org/10.1016/j.jksus.2017.07.012.

[46] J.Z. Zhou, S. Huang, J. Sheng, J.Z. Lu, C.D. Wang, K.M. Chen, H.Y. Ruan, H.S. Chen, Effect of repeated impacts on mechanical properties and fatigue fracture morphologies of 6061-T6 aluminum subject to laser peening, Mater. Sci. Eng. A. 539 (2012) 360–368. https://doi.org/10.1016/j.msea.2012.01.125.

[47] K.L. Murty, Materials Ageing and Degradation in Light Water Reactors: Mechanisms and management, Woodhead Publishing Ltd (2013).

[48] A. Bhaduri, Mechanical Properties and Working of Metals and Alloys, Springer (2018).

[49] I. Machlin, R.T. Begley, E.D. Weisert, Refractory metal alloys-Metallurgy and Technology, Plenum Press (1968).

[50] P. Lan, J.L. Meyer, J. Economy, A.A. Polycarpou, Unlubricated Tribological Performance of Aromatic Thermosetting Polyester (ATSP) Coatings under Different Temperature Conditions, Tribol. Lett. 61 (2016) 1–14. https://doi.org/10.1007/s11249-015-0621-3

[51] Y. Hua, Z. Rong, Y. Ye, K. Chen, R. Chen, Q. Xue, H. Liu, Laser shock processing effects on isothermal oxidation resistance of GH586 superalloy, Appl. Surf. Sci. 330 (2015) 439–444. https://doi.org/10.1016/j.apsusc.2015.01.033.

[52] H. Yang, X. Wu, G. Cao, Z. Yang, Enhanced boronizing kinetics and high temperature wear resistance of H13 steel with boriding treatment assisted by air blast shot peening, Surf. Coatings Technol. 307 (2016) 506–516. https://doi.org/10.1016/j.surfcoat.2016.09.029.

[53] A. Pauschitz, M. Roy, F. Franek, Mechanisms of sliding wear of metals and alloys at elevated temperatures, Tribol. Int. 41 (2008) 584–602. https://doi.org/10.1016/j.triboint.2007.10.003.

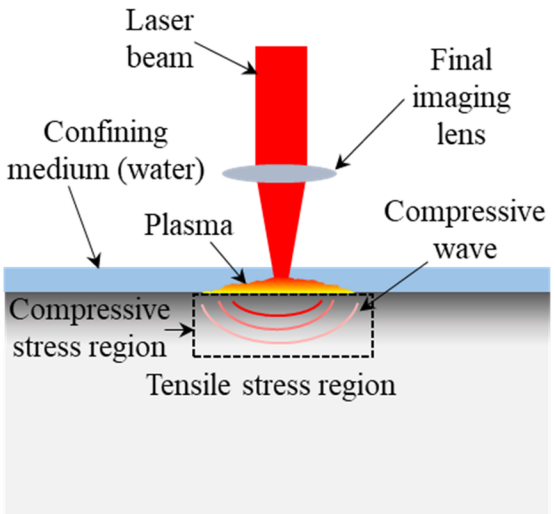
Laser beam
Final imaging lens
Confining medium (water)
Plasma
Compressive wave
Compressive stress region
Tensile stress region

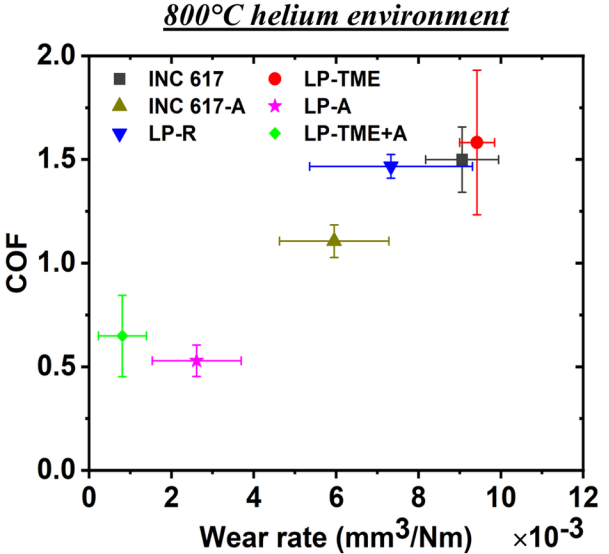
800°C helium environment
INC 617
INC 617-A
LP-R
LP-TME
LP-A
LP-TME+A
COF
Wear rate (mm3/Nm)
×10-3
0.0
0.5
1.0
1.5
2.0
0
2
4
6
8
10
12